Spiral drift and core properties

M. Wellner,[1,2] A. M. Pertsov,[1] and J. Jalife[1]
[1]*Department of Pharmacology, SUNY Health Science Center at Syracuse, Syracuse, New York 13210*
[2]*Physics Department, Syracuse University, Syracuse, New York 13244-1130*
(Received 9 November 1998)

We consider the drift of a stable, nonmeandering rotating spiral wave in a singly diffusive FitzHugh-Nagumo medium with generic reaction functions; the drift is assumed to be caused by a weak time-independent diffusivity gradient or convection term in the fast-variable equation. We address, to first order in the perturbation, the standard problem whose statement reads, ''Given the unperturbed solution, as well as the model's parameters, predict the speed and direction of the drift in terms of the strength and direction of the perturbation.'' Our main results are as follows: First, we establish a mathematical equivalence between true gradients and convective perturbations; second, a variety of numerical examples, taken from computer simulations, are presented as a reference base for testing drift theories; and third, we propose a semiempirical solution to the drift problem, requiring only two quantities to be measured off the unperturbed spiral, namely, its period of rotation and the value of the fast variable at its center; good agreement with numerical simulations is found for moderately sparse spirals. [S1063-651X(99)16705-9]

PACS number(s): 82.40.Ck

I. INTRODUCTION

Excitable media derive much of their interest from the varied and sometimes unexpected spatiotemporal wave patterns that they support, owing to their nonlinearity. Many such patterns have eluded analytical understanding. A medium that is obstacle-free, uniform, and isotropic can nevertheless exhibit robust spiral waves (in two dimensions) and scroll waves (in three dimensions). These phenomena form the subject of an extensive and still-growing literature; as a review, see [1,2]. Cardiac tissue is an important and well-recognized example of an excitable medium; it frequently displays spirals in pathological cases [3,4]. Here we single out a peculiar feature of spiral waves, namely, their behavior under a time-independent gradient in the medium's properties, or under the application of a time-independent field of some sort. Under these conditions it is well known [5–7] that, simultaneously with its rotation, the spiral has a drifting motion that can be uniform in speed and direction. Spiral drift is found in heart tissue [3–5]; sometimes it may be spontaneous (due to meandering [8,9]), and sometimes it may be gradient-induced [5]. Predictability of the drift could some day provide an avenue towards termination of the spiral wave.

One aim of this paper is to present, for theory-building purposes, some numerical examples of drift. We use a computationally simple model, amounting to a pair of generic FitzHugh-Nagumo (FHN) equations with single diffusivity. By varying its parameters we obtain a fair variety of behaviors, which we can hope are in some sense representative, and which to our knowledge do not substantially overlap with what exists in the literature.

Another aim is to propose a semiempirical rule for predicting the drift on the basis of the unperturbed spiral; the latter is assumed to be free of meandering. The problem we address is: Given an isotropic uniform medium, given a small constant vector $\mathbf{G}$ to represent the external perturbation, and given the unperturbed spiral solution (i.e., corresponding to $\mathbf{G}=0$), we want to predict the velocity of drift in magnitude and direction. This we may consider to be the standard drift problem, for which no practical solution has been available so far. We shall attempt to supply a partial answer.

If drift predictions are ever to become useful, it is essential that they should need minimal data from the unperturbed case. In our method only the value of the fast variable (defined below) at the center of rotation, as well as the period of rotation, are needed besides the strength of the perturbation and the parameters of the model. The proposed rule is based on representing the variables in the core by linear functions of the distance from the center of rotation. Such a point of view appears to be applicable when the core is neither too large (for example, with a totally unexcited area at the center) nor too small (with the action potential's nonlinear regime starting practically at the center); and indeed we shall demonstrate its serviceability in that range. Such moderately sparse spirals are encountered in cardiac tissue (see Fig. 8 in Ref. [4]), although some caution needs to be exercised in judging whether a spiral's sparsity is real or apparent (cf. Sec. IV further on).

Why should the behavior at the origin be relevant to spiral dynamics? The spiral's tip is generally considered to be a more plausible region in which to look for an explanation of reentrant activity. However, if the core is not too large, the oscillations close to the center are themselves due to tip behavior, and therefore, they may extract from the tip some information relevant to the drift. Because of the simplicity of such an approach, it will be worthwhile to look for any regularities in a comparison of the unperturbed center with drift features under perturbation.

Some earlier work done for the purpose of elucidating the mechanism of nonmeandering drift under a time-independent perturbation may be found in [10–13]. The present method does not overlap much with those studies. On the other hand, recent theoretical motivation for the core-based approach is to be found in the work of Biktashev and collaborators

[14,15]. They introduce spatial ''response functions'' whose knowledge allows one to determine the effect of a perturbation on a spiral; these functions depend only on the unperturbed spiral, and rotate together with it. To our knowledge, it seems that no simple method has been developed so far to calculate the response functions. For our purpose, however, their important feature is that they can decay rapidly in space, a fact verified in [15] for Ginzburg-Landau spirals. Thus, one may expect that some characteristics of the unperturbed core, and in some cases even its center, will be predictive of the perturbation-induced drift.

Unless otherwise noted, our discussion is based on the following equations for the propagating variables u (the fast variable) and v (the slow variable) in space $\mathbf{r}=(x,y)$ and time t:

$$\partial_t u - \mathcal{D}u + \Phi(u,v) = 0, \tag{1}$$

$$\partial_t v + \Psi(u,v) = 0, \tag{2}$$

where spatial propagation is entirely due to the differential operator,

$$\mathcal{D} = \alpha\nabla^2 + \mathbf{G}\cdot\boldsymbol{\nabla}. \tag{3}$$

In these equations Φ and Ψ are the reaction functions; in Appendix A we specialize them to produce our illustrations [16]. The diffusivity $\alpha>0$ and the vector $\mathbf{G}$ are fixed parameters. The problem of drift may now be stated as follows: If the reaction functions Φ and Ψ are given in detail, and if the unperturbed spiral solution is known, as well as the perturbation $\mathbf{G}$, one must predict the drift velocity vector $\mathbf{V}$.

Several remarks are in order about Eqs. (1)–(3). The form of $\mathcal{D}$, Eq. (3), corresponds to the external application of a constant uniform field $\mathbf{G}$, of undetermined physical nature but with well-defined effect on the waves. We also note that $\mathbf{G}$ has dimensions of velocity. For this reason it may be called a convection field; another reason is that if $-\mathbf{G}\cdot\boldsymbol{\nabla}v$ is added to the left side of Eq. (2) just as $-\mathbf{G}\cdot\boldsymbol{\nabla}u$ is already included in Eq. (1), then $\mathbf{G}$ correspond to a true convection (motion of the medium as a whole) in direction $-\mathbf{G}$, and the drift is a trivial one with velocity $-\mathbf{G}$. Even in the present paper, where convection occurs only in the first equation, we find some preponderance of drifting in the $-\mathbf{G}$ direction.

Any solution to the drift problem, as stated above, applies more generally than might appear from Eqs. (1)–(3). First suppose that Eqs. (1) and (2) contain the terms $\mathbf{G}\cdot\boldsymbol{\nabla}u$ and $\mathbf{G}'\cdot\boldsymbol{\nabla}v$,respectively. Then, as was pointed out in [12], an equivalent replacement for these two convection vectors is $\mathbf{G}\rightarrow\mathbf{G}-\mathbf{G}'$, $\mathbf{G}'\rightarrow 0$, implemented by transforming to a coordinate system with velocity $-\mathbf{G}'$. Thus the two-convection case is reduced to the single-convection case studied here.

Next, and more interesting in practice, consider a problem where the medium's diffusivity exhibits a spatial gradient. Without a gradient, a convection $\mathbf{G}\neq 0$ will only break the isotropy of the medium but not its uniformity; this is an important simplicity feature. If, however, the convective term is replaced by a gradient $\mathbf{G}$ in the diffusivity, the term $\mathcal{D}u$ should be the divergence of a current,

$$\mathcal{D}_{\mathrm{gr}}u = \boldsymbol{\nabla}\cdot[(\alpha+\mathbf{G}\cdot\mathbf{r})\boldsymbol{\nabla}u] \tag{4}$$

or, equivalently,

$$\mathcal{D}_{\mathrm{gr}}u = (\alpha+\mathbf{G}\cdot\mathbf{r})\nabla^2 u + \mathbf{G}\cdot\boldsymbol{\nabla}u, \tag{5}$$

a nonuniform situation, which therefore seems more complicated. Fortunately, as we demonstrate in Sec. II, gradient and convection are equivalent up to a conformal space mapping, at least to first order in the perturbation. Accordingly, in this paper we only need to postulate Eq. (1) with $\mathcal{D}$ given by Eq. (3).

A more general remark (also within the first-order perturbation context) is called for at this stage. The perturbing gradients discussed in the literature typically do not affect the diffusivity, but rather some other property of the medium such as the excitability or, indirectly, the spiral period. In those situations the spiral has been observed [20] to drift towards regions of longer period. If, on the their hand, we just have a gradient in the diffusivity, then there is zero gradient in the period, since the diffusivity controls the spatial but not the temporal scale. This is consistent with the fact that here the drift problem can be reduced to a convection problem where the medium is uniform. However, even though the period no longer depends on location, a nonzero drift still exists. Therefore, some agency in addition to the period gradient must be a cause of drift.

We should also mention some applications to cardiac excitation waves. These are affected by the following instances of diffusivity gradients: (a) Infarcted heart tissue has a reduced speed of wave propagation [17] and, in terms of models such as Eqs. (1)–(3), probably involve a reduced diffusivity. Thus, some regions of the heart would have a diffusivity that varies in space. (b) Healthy heart tissue displays a preferential direction of wave propagation, namely, the direction of greatest speed. That direction varies rather gradually across the heart wall, following the local orientation of the muscle fibers. This so-called twisted anisotropy causes a class of scroll waves to drift in a predictable way [18]. The analysis is carried out on the spiral resulting from a two-dimensional cross-section; the rotational anisotropy turns into a diffusivity gradient.

Induced spiral drift, although two dimensional, is relevant to three-dimensional problems. In particular, it is directly relevant to the shrinking and drifting of scroll rings [19–21], patterns in which the scrolls rotate around a quiescent ring-shaped filament. Here, the drift arises from a purely geometric effect, namely, the filament's curvature, which causes a convectivelike term to appear in the Laplacian of Eq. (1). [This term is nothing more than the $(1/r)\partial/\partial r$ introduced by cylindrical coordinates.] Any curved filaments, as are believed to occur in the heart under pathological conditions, will show a similar behavior. An adequate theory of drift would make that behavior quantitatively predictable, at least for filaments that are not excessively curved.

II. GRADIENT VERSUS CONVECTION

We first take care of the gradient problem by demonstrating its equivalence to the convection problem. Let the perturbation $\mathbf{G}$ be in the x direction for convenience. The claim is that, to first order in G, the differential operators of Eqs. (3) and (5),

$$\mathcal{D} = \alpha\nabla^2 + G\partial_x, \tag{6}$$

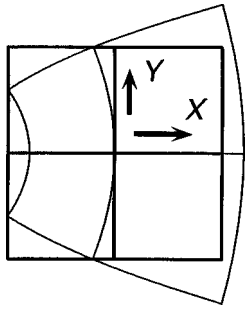

FIG. 1. An originally distorted pattern (fine lines) is made undistorted (thick lines) by the transformation of Eqs. (8) and (9). In this example we have $G/2\alpha=0.25$; the small undistorted squares have unit side.

$$\mathcal{D}_{\mathrm{gr}}=(\alpha+Gx)\nabla^2+G\partial_x, \tag{7}$$

are equivalent under a conformal space mapping. It is simplest to exhibit the results and verify its validity. In order to eliminate the term in x, we apply a quadratic coordinate transformation $(x,y)\rightarrow(X,Y)$ as follows:

$$X=x+\frac{G}{4\alpha}(-x^2+y^2), \tag{8}$$

$$Y=y-\frac{G}{2\alpha}xy. \tag{9}$$

Figure 1 shows that, relative to the origin, any pattern is enlarged or reduced in regions of positive or negative x, respectively. To first order in G we have,

$$\partial_x=\partial_X-\frac{G}{2\alpha}(X\partial_X+Y\partial_Y), \tag{10}$$

$$\partial_y=\partial_Y+\frac{G}{2\alpha}(Y\partial_X-X\partial_Y), \tag{11}$$

$$\nabla^2=\left(1-\frac{G}{\alpha}X\right)\nabla'^2, \tag{12}$$

where

$$\nabla'=(\partial_X,\partial_Y). \tag{13}$$

Hence, in Eq. (7), and noting that $x=X+o(G^2)$, we have

$$\begin{aligned}(\alpha+Gx)\nabla^2&=\alpha\left(1+\frac{G}{\alpha}X\right)\left(1-\frac{G}{\alpha}X\right)\nabla'^2+o(G^2)\\&=\alpha\nabla'^2+o(G^2).\end{aligned} \tag{14}$$

To first order in G, there is no term in X, and thus uniformity has been restored. Equations (8) and (9) represent the only quadratic transformation (up to a space translation) that will achieve this result. Indeed, they can be obtained deductively by trying the most general quadratic coordinate transformation, and requiring a result of the form (6). The remaining anisotropy $G\partial_x u$ will suffer only corrections of $o(G^2)$, and thus remains unaffected in the present treatment. This term is, of course, the essential part of the perturbation.

The transformation (8), (9) turns out to be conformal. This is most easily seen from a complex linear combination of Eqs. (8) and (9):

$$X+iY=(x+iy)-\frac{G}{4a}(x+iy)^2, \tag{15}$$

an analytic mapping of one complex plane into another. No analyticity of u or v is implied or assumed.

To summarize this section: We have shown that the nonuniform scaling effect of a small uniform diffusivity gradient can be removed by a purely spatial transformation; hence, the gradient can be reduced to its convective part. With regard to drifting mechanisms, we are led to the important conclusion that, to first order in the perturbation, nonuniform scaling without convection does not cause spiral drift. (Highly nonuniform situations can be very different in this respect, however, as in cases of boundaries or interfaces.)

III. OBSERVED DRIFT VELOCITIES

We have simulated the drifting spiral in a model whose reaction functions are specified in Appendix A. In all simulations, we have chosen clockwise rotating spirals, in conformity with much of the existing literature. The resulting drift velocity is a constant vector **V** pointing at a counterclockwise (i.e., positive) angle Γ to the perturbation **G**. Making the rotation counterclockwise changes the sign of Γ. We have varied three parameters, denoted by K_2, ϵ, and S_1. Here, K_2, the slope of the middle (unstable) segment of the piecewise linear Φ nullcline, controls the excitability of the medium; ϵ, which occurs as a factor in Ψ, controls the ratio of the main time constants of u and v; and S_1 controls the speed of recovery when the system is near its resting point. Our exploration of the parameter space is described in detail in Appendix A; the selected values have been subjected to the following criteria: (a) a sufficient amount of the spiral should fit inside the space lattice; (b) the unperturbed spiral should not meander; (c) each parameter should go through a set of approximately equidistant values; (d) a good variety of spiral features should be sampled; and (e) the conditions needed to initiate the spiral should be reasonably robust.

Figure 2 displays the normalized drift velocity vectors $\mathbf{V}/G$ in a range of parameter values. Each of the three parameters produces its own ''fan'' of such vectors as it is being varied; only the K_2 fan is being shown as an illustration. In order not to crowd the picture we draw only the outer vectors of the fan. In this and all other cases we have found the drift vector to lie in the upper half plane ($0<\Gamma<\pi$), or, in more general terms, the drift angle relative to the perturbation is opposite to the spiral's direction of rotation. Thus, with our chirality convention, **V** is always in the upper half plane. More specifically, the smallest observed drift angles approach 60° (Fig. 2), while the largest seem to approach 180°. For a numerical synopsis see Table II of Appendix A. The velocity's magnitude has not been seen to dip below a factor of roughly 0.4 of the perturbation strength. The observed drift velocities are listed numerically in Table II of Appendix A.

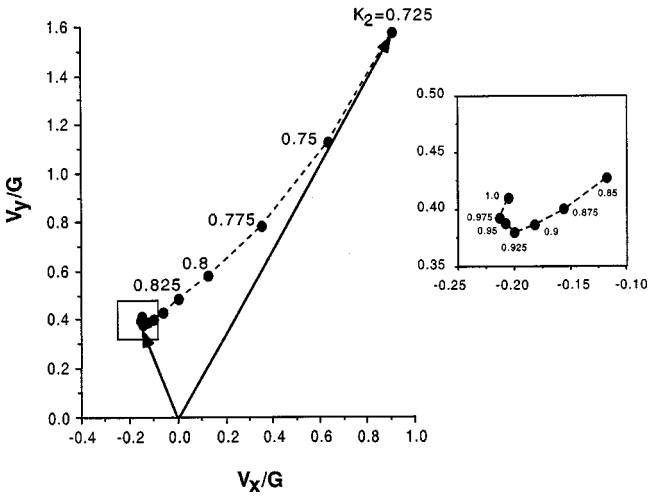

FIG. 2. Normalized drift velocity vectors $\mathbf{V}/G$ corresponding to the variation of a model parameter, K_2. Each range gives rise to a fan. Here only the outer vectors are drawn in full; the values of K_2 are indicated. This fan appears bounded by a 60° asymptote and a 120° tangent. Nowhere have we observed any drift angle less than 60°. The inset magnifies the crowded region. All vectors in this article's survey lie in the upper half plane, and their magnitudes are comparable to unity.

IV. RELATION BETWEEN DRIFT AND DENSITY

The density of a spiral turns out to be relevant to our study in two different ways. First, dense spirals tend to drift against the perturbation ($\mathbf{V}\cdot\mathbf{G}<0$), while the opposite tends to be the case for sparse spirals; this agrees with an earlier observation by Krinsky and collaborators [12]. Second, as discussed in Sec. VII further on, the accuracy of our own formulas requires a moderate density. In Fig. 3(a) we test the qualitative density-drift relation by plotting all observed densities σ against the normalized drift-velocity component V_x/G in the direction of perturbation. The dependence is nearly monotonic, even in the intermediate density range not addressed by Ref. [12].

In the above, we define the density in terms of the outer turns of the spiral as follows:

$$\sigma=\frac{\text{(total width of an isolated pulse)}}{\text{(cycle wavelength)}}. \tag{16}$$

The total pulse width is measured between cutoff amplitudes chosen very close to the resting point. Here we choose a cutoff $u_c=(0.1)A_1$, where A_1 is the minimum of the nullcline for u, see Appendix A. The cutoff for v can then be defined without too much arbitrariness in terms of the other nullcline, $\Psi(u_c)=0$. Thus, numerically, we have $u_c=v_c=0.0018$. Keeping in mind that here the resting point is at $u=v=0$, we begin the pulse where its magnitude rises to $|u|=u_c$ or $|v|=v_c$, whichever comes first, and we end it correspondingly; see the first inset of Fig. 3(a). When the pulses are close together, we measure the total width at a pacing frequency lower than that of the spiral, so as to detach the pulses from one another. (Once they are well separated the precise value of the pacing frequency does not affect their width.) Densities measured in this way are listed in Table I for all simulations considered here. The density is

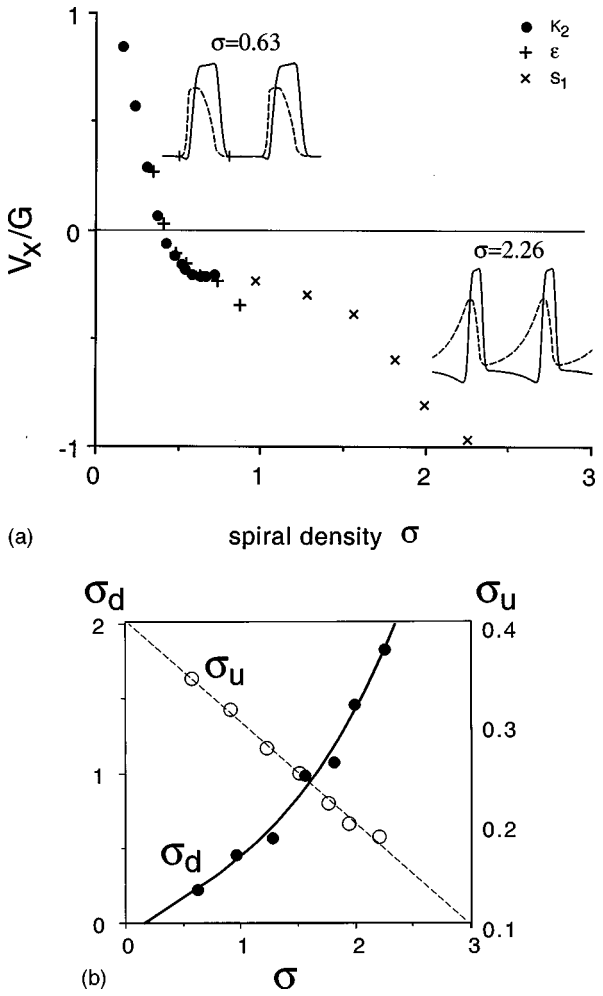

FIG. 3. (a) Drift velocity to the right is inversely correlated with the density σ. From left to right, the extreme values of K_2 are 0.725 and 1, the extremes of ϵ are 2 and 0.5, and the extremes of S_1 are 0.5 and 12.5; see Table II for this figure's data. The insets are examples of sparse (top) and dense (bottom) radial dependences of the spiral arms; the wave forms are u (solid) and v (dashed). (b) This panel illustrates the importance of a careful definition of density. In the S series of simulations, an alternative density σ_u, obtained from the half-amplitude points of the u pulse, is inversely correlated with our definition; on the other hand, the more fundamental, dispersion-based definition σ_d of Eq. (17) correlates excellently with σ.

greater than one for crowded pulses, which can therefore be thought of as ''overlapping''; it is equal to one for barely colliding pulses, and less than one for detached pulses. The more often seen definition of pulse width, in terms of the half-maximal amplitude of the variable u only, does not work very well in the density-drift relation. To display that fact we show in Fig. 3(b) that those two definitions are inversely correlated in the S series of simulations, where the recovery period is long. (In these simulations it would make little practical difference to ignore the cutoff of v and only compare $|u|$ to $u_c=0.0018$.) Further on in this paper we discuss the predictive inaccuracy that occurs under extreme densities.

In order to confirm the appropriateness of our definition in the S series, we ask whether σ correctly reflects the interaction between successive turns of the spiral: a pulse's speed c

is less when its front feels the preceding pulse's tail. Thus, for denser waves, c becomes more sensitive to the cycle wavelength, and hence to the period τ. On the basis of this dispersion property, it is natural to set

$$\sigma_d = \frac{c_\infty - c}{c - c_{\rm cr}}, \tag{17}$$

where c_∞, c, and $c_{\rm cr}$ are the plane-wave speeds at infinite period, spiral period, and minimum sustainable (critical) period, respectively. This model-independent criterion, which furthermore does not require inspection of the slow variable v, correlates very well with σ; see Fig. 3(b).

V. UNPERTURBED CORE CENTER

As a possible strategy for predicting drift behavior, we begin by observing the nonmeandering unperturbed spiral at the location where it is simplest to describe, namely, the center of its core, i.e., the center of rotation. At that point, which we take as the origin of space coordinates, both propagating variables are constant in time and, in this paper, equal to each other as pointed out below. We assume the core is not too large; more specifically, it does not possess a resting area, where $u=u_0$, $v=v_0$, overlapping the origin. On the basis of only two measurements taken off the spiral, namely, the fast variable u_0 at the center and the spiral's rotation period τ, we now determine, near the origin, the relative phases of several oscillating quantities, u, v, $\partial_t u$, $\partial_t v$, $-\mathcal{D}u$, Φ, and Ψ, which occur in the FHN equations; some of these phases are nontrivial.

In the following we use Cartesian and polar coordinates (x,y) and (r,θ). There is not loss of generality in taking $G_x=G$, $G_y=0$. We assume that u and v have a double power series expansion in x and y within at least a small disc around the origin. In polar coordinates, and with rigid rotation at angular velocity ω around the origin, this leads to

$$u = u_0 + u_1 r\cos(\theta+\omega t) + o(r^2), \tag{18}$$

$$v = v_0 + v_1 r\cos(\theta-\psi+\omega t) + o(r^2), \tag{19}$$

where $u_1>0$ and $v_1>0$ are constants; we choose a zero phase for u at $t=0$ and $\theta=0$, and ψ is the phase lag of v relative to u. (The use of complex amplitudes appears to have no advantages in the trigonometry that will be needed.) If u_0 and u_1 are measured, as well as ω, then v_0, v_1, and ψ are found analytically from the FHN Eqs. (1) and (2) by solving

$$\Psi(u_0,v_0)=0, \tag{20}$$

and by inserting Eqs. (18) and (19) into Eq. (2), requiring validity at all times. The result is $u_0=v_0$ for our class of models, and

$$u_1\partial_u\Psi\cos\psi + v_1\partial_v\Psi = 0, \tag{21}$$

$$u_1\partial_u\Psi\sin\psi + v_1\omega = 0. \tag{22}$$

Compatibility of Eqs. (21) and (22) means

$$\tan\psi = \omega/\partial_v\Psi. \tag{23}$$

We note that, in Eqs. (21) and (22), we have $\partial_u\Psi<0$, $\partial_v\Psi<0$ [cf. Appendix A, Eq. (A2)], and thus we have obtained the exact phase relation between u and v near the origin, with

$$0<\psi<\pi/2. \tag{24}$$

It should always be understood that $\partial_u\Phi$, $\partial_v\Phi$, $\partial_u\Psi$, and $\partial_v\Psi$ are evaluated at the origin, i.e., at $u=u_0$, $v=v_0$. Actually, in our family of simulations the value of u_0 is not very critical, owing to the piecewise linearity or piecewise constancy of the reaction functions. In our attempts to predict the drift we only deal with cases where $u_1<u_0<u_2$, $B_1<u_0<B_2$, so that we have [cf. Appendix A]

$$\partial_u\Phi=-K_2,\quad \partial_v\Phi=1,\quad \partial_u\Psi=-\epsilon/S_2,\quad \partial_v\Psi=\epsilon/S_2. \tag{25}$$

In the remaining part of this section we linearize the FHN equations themselves near the origin for $G=0$. [From here on we omit the mention ''$+o(r^2)$'' unless needed for clarity.] Consider first the left side of Eq. (1). Similarly to the linearization of u and v, shown above, we introduce a parametrization,

$$\partial_t u = Ar\cos(\theta-\chi_A+\omega t), \tag{26}$$

$$-\mathcal{D}u = (-\mathcal{D}u)_0 + Br\cos(\theta-\chi_B+\omega t), \tag{27}$$

$$\Phi(u,v) = \Phi(u_0,v_0) + Cr\cos(\theta-\chi_c+\omega t). \tag{28}$$

Applying $\boldsymbol{\nabla}$ to Eq. (1) yields the three real vectors $\mathbf{A}(t)=\nabla\partial_t u$, $\mathbf{B}(t)=\boldsymbol{\nabla}(-\mathcal{D}u)$, and $\mathbf{C}(t)=\nabla\Phi$, evaluated at the origin. They have constant magnitudes A, B, and C, and rotate clockwise with angular velocity ω; their phases at $t=0$ are χ_A, χ_B, and χ_C. The $o(r)$ term of the unperturbed Eq. (1) now amounts to

$$\mathbf{A}+\mathbf{B}+\mathbf{C}=0. \tag{29}$$

Equation (29) says that vectors **A**, **B**, and **C** form a (rotating) triangle. That triangle, shown further on in Fig. 4, is a visual representation of the activity at the center of a spiral, and we next determine its shape, starting from a knowledge of the unperturbed quantities u_0 and ω.

Vector **A**: Comparison of Eqs. (18) and (26) gives

$$\chi_A=-\pi/2,\quad A=\omega u_1. \tag{30}$$

Vector **C**: Eq. (28), after expansion of the left side, gives for the coefficients of r:

$$\partial_u\Phi u_1\cos(\theta+\omega t) + \partial_v\Phi v_1\cos(\theta-\psi+\omega t) = C\cos(\theta-\chi_C+\omega t). \tag{31}$$

With the special value $\theta+\omega t=\chi_C+\pi/2$, and using Eq. (21), the above yields χ_C:

$$\cot\chi_C = \cot\psi - \frac{\partial_u\Phi\,\partial_v\Psi}{\partial_v\Phi\,\partial_u\Psi\sin\psi\cos\psi}; \tag{32}$$

the quadrant of χ_C is subject to $C>0$, see the next equation. Taking $\theta+\omega t=\pi/2$, we have from Eq. (31),

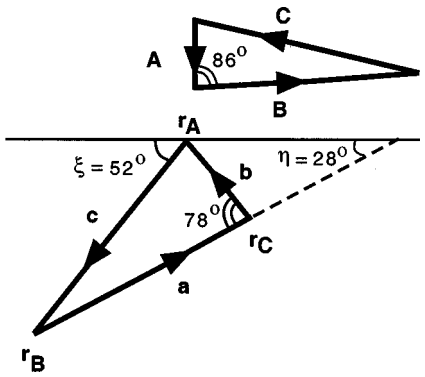

FIG. 4. The lower triangle **abc** is the ''drift triangle,'' illustrated for simulation ($\epsilon 1$). For example, vector **a** connects the perturbed rotation centers, in space, of the amplitude terms **B** and **C** shown in the upper triangle; similarly for the other vectors, see Eq. (63). Triangle **abc** does not rotate, while triangle **ABC** rotates clockwise and is shown here in its $t=0$ orientation. We observe a rough equality between angles **ab** and **AB** (inset); this is a useful rule for most simulations. (The isosceles nature of the present triangle **abc** is fortuitous.) Another useful rule results from observing that angles ξ and η add up to roughly $\pi/2$.

$$C=-\frac{\partial_v\Phi\,\partial_u\Psi\,\sin\psi\cos\psi}{\partial_v\Psi\,\sin\chi_C}u_1. \tag{33}$$

Vector **B**: From Eq. (29), with $\theta+\omega t=\chi_B+\pi/2$, we have

$$\tan\chi_B=\left[1+\frac{(\partial_v\Psi)^2}{\partial_v\Phi\,\partial_u\Psi\cos^2\psi}\right]\tan\chi_C, \tag{34}$$

in which the quadrant of χ_B is subject to $B>0$ in the expression below. With $\theta+\omega t=\chi_C+\pi/2$, we have

$$B=\frac{\omega\cos\chi_C}{\sin(\chi_B-\chi_C)}u_1. \tag{35}$$

The following identity will be of some use in Appendix C:

$$\partial_v\Phi\,\partial_u\Psi=-\frac{\omega^2\cos\chi_B\sin\chi_C}{\sin(\chi_C-\chi_B)}; \tag{36}$$

it follows from combining the sine rule for C/A with Eqs. (33) and (22). The internal angles of triangle **ABC**, modulo 2π, are

$$\angle\mathbf{AB}=\pi+\chi_A-\chi_B \quad \text{and cyclic permutations,} \tag{37}$$

all positive if the sequence **ABC** is counterclockwise, all negative in the opposite case; see Fig. 4 further on for an example.

Having expanded Eq. (1) at the origin, we now treat Eq. (2) similarly:

$$\partial_t v=Pr\cos(\theta-\chi_P+\omega t), \tag{38}$$

$$\Psi(u,v)=\Psi(u_0,v_0)-Pr\cos(\theta-\chi_P+\omega t). \tag{39}$$

This involves a vector $\mathbf{P}=\boldsymbol{\nabla}\partial_t v=-\boldsymbol{\nabla}\Psi$ with magnitude P and phase χ_P at $t=0$, where

$$P=\omega v_1, \quad \chi_P=\psi-\pi/2; \tag{40}$$

see Eq. (19).

Summarizing this section: We have obtained the phase shift ψ that exists between the propagating variables near the center of the unperturbed spiral. We have also constructed the rotating amplitude triangle **ABC** involving the individual terms of the first FHN equation, and the rotating amplitude vectors **P**, $-\mathbf{P}$ for the terms of the second FHN equation.

VI. PERTURBED CORE CENTER

We next rewrite the perturbed FHN Eqs. (1), (2), and (3) in the codrifting system, which is postulated to have uniform velocity **V**. The time derivative now acquires a convective term, $\partial_t\rightarrow\partial_t-\mathbf{V}\cdot\boldsymbol{\nabla}$, and the equations read

$$\partial_t u-(\mathbf{V}+\mathbf{G})\cdot\boldsymbol{\nabla}u-\alpha\nabla^2u+\Phi(u,v)=0, \tag{41}$$

$$\partial_t v-\mathbf{V}\cdot\boldsymbol{\nabla}v+\Psi(u,v)=0. \tag{42}$$

The codrifting system may be said to define **V**, rather than vice-versa. The definition amounts to the following requirement: In the codrifting system, the perturbed spiral must have a unique fundamental frequency ω_{pert}, independent of space and time.

It will be of considerable use to note that the perturbed frequency $\omega_{\text{pert}}(G)$ is unchanged from the unperturbed value, at least to $o(G)$; this is readily seen from symmetry. Indeed, consider, in general, a perturbed frequency $\omega_{\text{pert}}=\omega_{\text{pert}}(G)$. We express the vector **G** as $\mathbf{G}=G\mathbf{n}_x$, where $\mathbf{n}_x$ is the unit vector in the x direction, and make the transformation $G\rightarrow-G$, equivalent to

$$\mathbf{G}\rightarrow-\mathbf{G}. \tag{43}$$

Another way to implement Eq. (43) is to rotate coordinates by 180°. This (passive) rotation cannot affect the physics and, therefore, cannot affect any permanent scalar feature of the spiral, such as its frequency. Thus we have $\omega_{\text{pert}}(G)=\omega_{\text{pert}}(-G)$, leading to

$$\omega_{\text{pert}}=\omega+o(G^2). \tag{44}$$

Transformation (43) will of course reverse **V** and change the spiral's phase by 180°.

The present section leads to the following geometrical result concerning the perturbed versions of the rotating amplitude vectors in the codrifting system: The centers of rotation of u and v become distinct; the same can be said of the centers about which the other amplitudes **A**, **B**, **C**, and **P** rotate. In that system, the centers form a static cluster, $o(G)$ in extent; the origin of codrifting coordinates will be chosen within that cluster, i.e., at an $o(G)$ distance of any of these points. We shall pay special attention to a triangle, **abc**, formed by the rotation center of the terms **A**, **B**, and **C** in Eq. (1). A special case of that triangle will be shown in Fig. 4.

As an illustration, we find a center $\mathbf{r}_u$ for u by considering its fundamental frequency component u_ω and defining $\mathbf{r}_u$ as the point where that component has zero amplitude. The $o(G)$ correction term for u at $\mathbf{r}=0$ can be denoted without loss of generality by

$$\delta u=-u_1r_u\cos(\omega t+\theta_u). \tag{45}$$

To $o(G)$, there are no harmonics (frequencies 2ω, 3ω, ...) at the origin, nor is there any zero-frequency correction at that point. Appendix B demonstrates the validity of these statements, as well as the geometrical meaning of the constant parameters (r_u, θ_u): they are the polar coordinates of $\mathbf{r}_u$. A similar parametrization can be used for $\mathbf{r}_v$. Returning to Eqs. (41) and (42), and keeping in mind the notation of Eqs. (26)–(28), as well as Eqs. (38) and (39), we similarly have the corrections,

$$\delta(\partial_t u) = -Ar_A \cos(\omega t - \chi_A + \theta_A) = -\mathbf{A}\cdot\mathbf{r}_A, \quad (46)$$

$$\delta(-\alpha\nabla^2 u) = -Br_B \cos(\omega t - \chi_B + \theta_B) = -\mathbf{B}\cdot\mathbf{r}_B, \quad (47)$$

$$\delta\Phi = -Cr_C \cos(\omega t - \chi_C + \theta_C) = -\mathbf{C}\cdot\mathbf{r}_C, \quad (48)$$

$$\delta(\partial_t v) = -Pr_P \cos(\omega t - \chi_P + \theta_P) = -\mathbf{P}\cdot\mathbf{r}_P, \quad (49)$$

$$\delta\Psi = +Pr_Q \cos(\omega t - \chi_P + \theta_Q) = +\mathbf{P}\cdot\mathbf{r}_Q, \quad (50)$$

where the fixed vectors $\mathbf{r}_A$, $\mathbf{r}_B$, $\mathbf{r}_C$, $\mathbf{r}_P$, and $\mathbf{r}_Q$, with phases θ_A, θ_B, θ_C, θ_P, and θ_Q represent the individually shifted rotation centers of these five terms. We also need the $\mathbf{V}$ and $\mathbf{G}$ terms in Eqs. (41) and (42), keeping in mind that they require the unperturbed values of $\nabla u, \nabla v$ taken from Eqs. (18) and (19). We have

$$(\mathbf{V}+\mathbf{G})\cdot\nabla u = u_1[V\cos(\omega t + \Gamma) + G\cos\omega t] = (\mathbf{V}+\mathbf{G})\cdot\mathbf{u}_1, \quad (51)$$

$$\mathbf{V}\cdot\nabla v = v_1 V \cos(\omega t + \Gamma) = \mathbf{V}\cdot\mathbf{v}_1, \quad (52)$$

where $\mathbf{u}_1$ has magnitude u_1 and phase zero at $t=0$; $\mathbf{v}_1$ has magnitude v_1 and phase ψ at $t=0$; both vectors rotate clockwise at angular frequency ω. The $o(G)$ correction to the FHN equations (41) and (42) now reads

$$\mathbf{A}\cdot\mathbf{r}_A + \mathbf{B}\cdot\mathbf{r}_B + \mathbf{C}\cdot\mathbf{r}_C = -(\mathbf{V}+\mathbf{G})\cdot\mathbf{u}_1, \quad (53)$$

$$\mathbf{P}\cdot(\mathbf{r}_P - \mathbf{r}_Q) = \mathbf{V}\cdot\mathbf{v}_1, \quad (54)$$

with fixed $\mathbf{r}_P, \mathbf{r}_Q$. Two more $o(G)$ constraints can be obtained from the details of the reaction functions Φ, Ψ. Expansion of these functions at the origin yields

$$\mathbf{C}\cdot\mathbf{r}_C - (\partial_u\Phi)\mathbf{u}_1\cdot\mathbf{r}_A - (\partial_v\Phi)\mathbf{v}_1\cdot\mathbf{r}_P = 0, \quad (55)$$

$$\mathbf{P}\cdot\mathbf{r}_Q + (\partial_u\Psi)\mathbf{u}_1\cdot\mathbf{r}_A - (\partial_v\Psi)\mathbf{v}_1\cdot\mathbf{r}_P = 0, \quad (56)$$

where

$$\mathbf{u}_1\cdot\mathbf{r}_A = u_1 r_A \cos(\omega t + \theta_A), \quad (57)$$

$$\mathbf{v}_1\cdot\mathbf{r}_P = v_1 r_P \cos(\omega t + \theta_P - \psi). \quad (58)$$

The set of Eqs. (53)–(56) should be invariant under space translation. Indeed, the origin of coordinates is unspecified except for the fact that is near (or in) the cluster of shifted rotation centers. The right sides of Eqs. (53) and (54) do not depend on the origin. Owing to Eq. (29), the left side of Eq. (53) is invariant under any translation $\mathbf{s}$: $\mathbf{r}_A \to \mathbf{r}_A + \mathbf{s}$, $\mathbf{r}_B \to \mathbf{r}_B + \mathbf{s}$, and $\mathbf{r}_C \to \mathbf{r}_C + \mathbf{s}$. The left side of Eq. (54) is manifestly invariant. To test Eq. (55) for translation invariance, we ask whether

$$[\mathbf{C} - (\partial_u\Phi)\mathbf{u}_1 - (\partial_v\Phi)\mathbf{v}_1]\cdot\mathbf{s} = 0 \quad (59)$$

for arbitrary $\mathbf{s}$, or

$$\mathbf{C} - (\partial_u\Phi)\mathbf{u}_1 - (\partial_v\Phi)\mathbf{v}_1 = 0. \quad (60)$$

Equation (59) is nothing but Eq. (31) with a phase $\omega t + \theta$ for $\mathbf{s}$. Similarly, invariance of Eq. (56) requires

$$[\mathbf{P} - (\partial_u\Psi)\mathbf{u}_1 - (\partial_v\Psi)\mathbf{v}_1]\cdot\mathbf{s} = 0 \quad (61)$$

for arbitrary $\mathbf{s}$, or

$$\mathbf{P} - (\partial_u\Psi)\mathbf{u}_1 - (\partial_v\Psi)\mathbf{v}_1 = 0. \quad (62)$$

Equation (61) is just Eq. (39) with the left side expanded.

We now consider that perturbed quantities need to be computed. Ultimately, we want to predict $\mathbf{V}$. Equations (53)–(56) involve the unknowns $\mathbf{r}_A$, $\mathbf{r}_B$, $\mathbf{r}_C$, $\mathbf{r}_P$, $\mathbf{r}_Q$, and $\mathbf{V}$. Translation invariance allows us to set one of the $\mathbf{r}$ vectors to zero, for example, $\mathbf{r}_A = 0$. Thus, we have four vector equations for five vector unknowns — insufficient information for a deductive determination of $\mathbf{V}$. Nevertheless, when $\mathbf{V}$ is supplied by an actual drift measurement, then the locations of all the shifted rotation centers can be found up to an overall translation. In particular, we can find the shape and orientation of the ''drift triangle,''

$$\mathbf{a} = \mathbf{r}_C - \mathbf{r}_B, \quad \mathbf{b} = \mathbf{r}_A - \mathbf{r}_C, \quad \mathbf{c} = \mathbf{r}_B - \mathbf{r}_A. \quad (63)$$

Its formal correspondence with the ''amplitude triangle'' **ABC** suggests that we look for some kind of similarity or transformation between the two. This we undertake in the next section.

We conclude the present section with a calculation of the drift triangle. The shifted centers $\mathbf{r}_P$, $\mathbf{r}_Q$, and $\mathbf{r}_C$, with $\mathbf{r}_A = 0$, are obtained rather simply from Eqs. (54)–(56) as follows:

$$\theta_P = \Gamma - \psi + \pi, \quad r_P = \frac{V\sin\psi}{\omega}, \quad (64)$$

$$\theta_Q = \Gamma - \psi - \pi/2, \quad r_Q = \frac{V\cos\psi}{\omega}, \quad (65)$$

$$\theta_C = \Gamma + \chi_C - 2\psi - \pi, \quad r_C = \frac{VP\partial_v\Phi\sin\psi}{\omega^2 C}; \quad (66)$$

after applying some trigonometry to Eq. (53) and setting

$$k = -\frac{\partial_v\Phi\,\partial_u\Psi\sin^2\psi}{\omega^2}, \quad (67)$$

we find θ_B from

$$\tan(\theta_B - \chi_B) = \frac{\sin\Gamma - k\sin(\Gamma - 2\psi)}{\cos\Gamma - k\cos(\Gamma - 2\psi) + G/V}, \quad (68)$$

subject to $r_B > 0$ below; we find r_B from

$$\frac{r_B}{G} = \frac{(u_1/B)[\sin(\Gamma - 2\psi) - (V/G)\sin 2\psi]}{\sin(\theta_B - \chi_B - \Gamma + 2\psi)}. \quad (69)$$

As an example we draw in Fig. 4 the drift triangle **abc** for simulation ($\epsilon 1$), corresponding to the amplitude triangle **ABC** calculated according to Sec. V and shown above it.

The results obtained in the present section have been as follows: the propagating variables, as well as the terms of the FHN equations, have been corrected to first order in the perturbation; each of these corrected quantities rotates about its own displaced center; the three centers involving the first FHN equation from a triangle **abc**, which is stationary and nonrotating in the codrifting coordinate system; we have determined the shape of this triangle on the basis of the observed spiral drift.

VII. SEMIEMPIRICAL RULES FOR THE DRIFT VELOCITY

The deductive results obtained so far do not in any way constrain the vector **V**. In order to supply the necessary information we study the drift triangle obtained from simulations, and as a result, we propose three constraints. We like to call them semiempirical rather than empirical, because they do not contain any adjustable parameters. The first rule deals with chirality, the second deals with the shape of the drift triangle, while the third involves information about its orientation.

A chirality rule. Comparing triangles in Fig. 4, we notice that both sequences **ABC** and **abc** occur with the same chirality (here counterclockwise). We adopt this as a rule, and shall use it in Appendix C to choose between several possible predictions.

A shape rule. Next, we can look for approximate angular equalities. Some, like that between angles **CA** and **bc**, are fortuitous — a fact borne out by surveying other cases. Similarly, the near equality $\angle\mathbf{ab}=\angle\mathbf{bc}$ (or $a=c$) appears coincidental. However, we do postulate an equality between the angles marked in both figures by a double arc,

$$\angle\mathbf{ab}=\angle\mathbf{AB}, \tag{70}$$

a natural observation in view of the mapping $\mathbf{A}\rightarrow\mathbf{a}$, $\mathbf{B}\rightarrow\mathbf{b}$, and $\mathbf{C}\rightarrow\mathbf{c}$. We turn Eq. (70) into a usable formula through the sine law, $[\sin(\angle\mathbf{ab})]/c=[\sin(\angle\mathbf{ca})]/b$, or

$$\frac{\sin(\angle\mathbf{ab})}{r_B}=\frac{\sin(\angle\mathbf{ab}-\theta_B+\theta_C)}{r_C}; \tag{71}$$

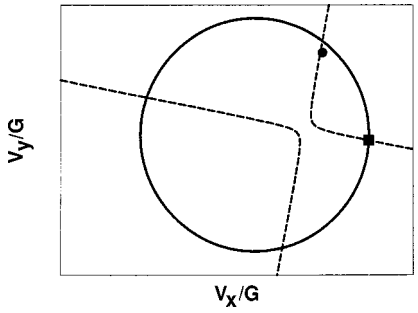

FIG. 5. Simultaneous requirement of the shape and orientation rules (cf. caption of Fig. 4) results in the intersection of a circle and a rectangular hyperbola in the $\mathbf{V}/G$ plane. Of the four available intersection points, we must choose the one on the upper right, as explained in Appendix C. The observed drift is shown as a small black circle. The square marks the origin. The illustration is for simulation ($\epsilon 1$).

Eq. (70) reads

$$\angle\mathbf{ab}=\pi+\chi_A-\chi_B=\pi/2-\chi_B\,. \tag{72}$$

Combining Eqs. (71) an (72), we have

$$\frac{\cos\chi_B}{r_B}=\frac{\cos(\theta_B-\theta_C+\chi_B)}{r_C}. \tag{73}$$

This is our formulation of the shape rule.

An orientation rule. We recall that triangle **ABC** rotates. However, **abc** is fixed in the codrifting system, and we search Fig. 3 for an approximate rule involving its orientation. In that figure, angles ξ and η add up to about $\pi/2$, a feature also found in a number of other simulations (not shown). We, therefore, postulate

$$\xi+\eta=\pi/2. \tag{74}$$

In Fig. 4, we have $\xi=\pi+\theta_B$ and $\angle\mathbf{ca}=\xi-\eta$, and, therefore, Eq. (74) amounts to

$$\angle\mathbf{ca}=2\theta_B+3\pi/2. \tag{75}$$

It must be noted that Eqs. (74) and (75) make no reference to triangle **ABC**, whereas the shape rule does. However, it will

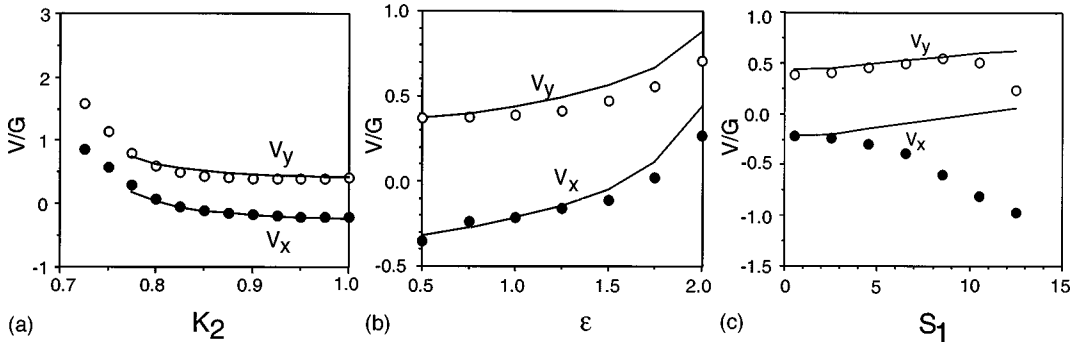

FIG. 6. Observed (points) and predicted (curves) values of the normalized components V_x/G, V_y/G. Panels (a), (b), and (c) illustrate the K, ϵ, and S series of simulations, respectively. In (a), there is no prediction corresponding to the first two values of K_2 because the spirals are supersparse or nearly so; see Fig. 8.

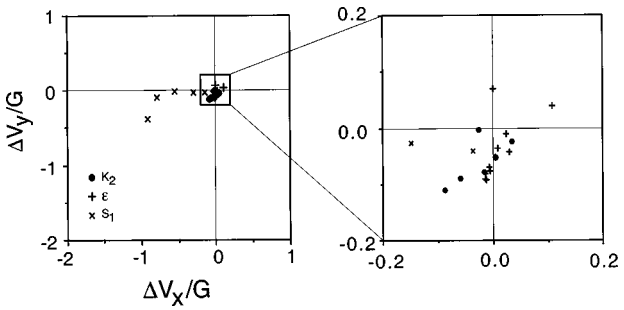

FIG. 7. Quality of the predictions. We plot [**V** (observed) $-$**V** (predicted)]/G. The small rectangle around the origin contains 18 points; the four others correspond to densities $\sigma>1.28$. See Sec. IV for the definition of σ.

be found advantageous to combine Eq. (75) with the shape rule expressed as Eq. (72). Summing the three internal angles to π gives

$$\theta_B+\theta_C=\chi_B-\pi. \tag{76}$$

This formula is a usable combination of the shape and orientation rules.

Combining the three rules results in a prediction of **V**. We display that vector in a coordinate plane ($V\cos\Gamma$,$V\sin\Gamma$). In this **V** plane, Eq. (73) can be shown to represent a circular locus, while Eq. (76) is a rectangular hyperbolic locus. We then find **V** as one intersection of these two curves. The algebra is sketched in Appendix C, which also discusses the choice of intersection among four possibilities. In our illustrative case, simulation (ϵ1), the intersecting loci are displayed in Fig. 5. The observed drift vector, shown here as well, is in this case close to the appropriate intersection. Predictions and observations are displayed in detail in Figs. 6 and 7. In most cases the agreement is good; the poor cases can be empirically related to the extreme density or sparsity of the spiral, as documented in Table II of Appendix A.

Finally, we consider the effect of extreme densities on the validity of the our semiempirical drift prediction. Figures 6 and 7 show that all densities $\sigma>1$ (to be found in the S series) give us poor predictions for V_x, getting worse as σ gets larger. These extreme points are outside the small box in Fig. 7. For very low densities, represented here by simulations (K.725) and (K.75), we cannot expect any prediction based on the core's center. Its near inactivity is indicated in Fig. 8.

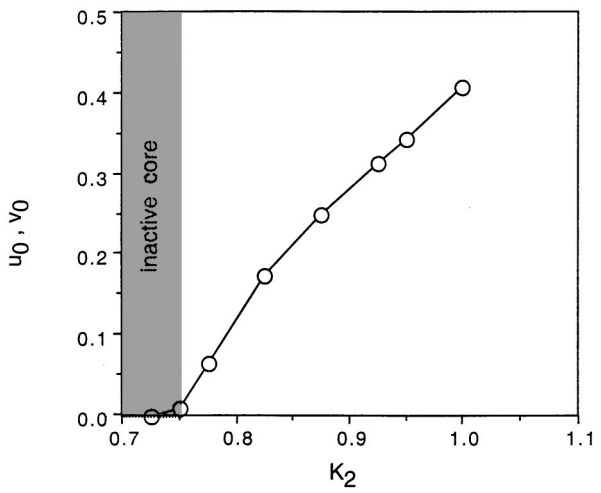

FIG. 8. Central value of u for the various K_2 values. Note the cases of vanishing u_0, combined with proximity to discontinuities at $u=A_1$ or $u=B_1$, which hinder our predictions in the shaded zone.

VIII. SUMMARY

We have considered the drift of a stable, nonmeandering rotating spiral wave in a singly-diffusive FitzHugh-Nagumo medium with generic reaction functions; the drift was assumed to be caused by a weak time-independent diffusivity gradient **G** or equivalent convection term in the fast-variable equation. We have addressed, to first order in the perturbation, the standard problem whose statement reads, ''Given the unperturbed solution, as well as the model's parameters, predict the speed and direction the drift in terms of the strength and direction of the perturbation.'' Our results are as follows: (a) We have presented a numerical survey of the spiral drift **V** under a perturbation **G** for a variety of model parameters. This part of the study is intended to serve as a reference base for testing drift theories. (b) We have established the equivalence, under a conformal space transformation, between true gradients and convective perturbations. (c) We have extended to intermediate spiral densities the observation that density is correlated with direction of drift: higher densities opposite to **G**, lower densities less so. (d) We have studied the simplest features of the unperturbed core in order to see how they might apply to the drifting core; among others, we have found the relative phase angle between the slow and fast variable at the center of rotation. (e) We have demonstrated that, under perturbation, that center splits up into a rigidly drifting cluster of rotation centers; also that the codrifting period of rotation is unchanged from the unperturbed one. (f) We have proposed a semiempirical solution to the drift problem, requiring only two quantities to be measured off the unperturbed spiral, namely, its period of rotation and the value of the fast variable at its center. The fact that only two easily measured unperturbed parameters are required makes the method a practical one. Good agreement with numerical simulations was found for spirals of intermediate densities. This range of validity is unusual for an approximate formula, in that it is not asymptotic. It can be understood qualitatively to some extent: at sufficiently low density the core is unexcited at the center, while at high density the spiral's outer turns might be expected to play a larger role.

ACKNOWLEDGMENTS

For useful conversations during the course of this work, we thank J. Beaumont and O. Berenfeld, as well as the latter for his valuable comments on the manuscript. Our research was supported by the National Blood and Heart Institute under Grant No. HL39707 and the American Heart Association under Grant-in-Aid No. 94016950.

APPENDIX A: DETAILS OF THE UNPERTURBED MODEL

The reaction functions [16] and parameters used in the numerical simulations are as follows. Referring to Eqs. (1)

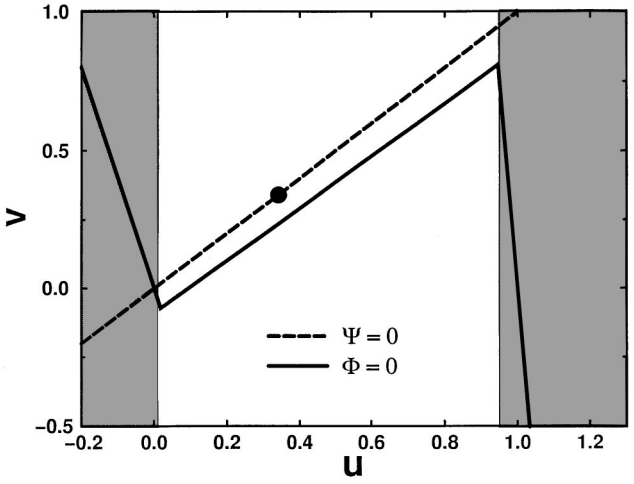

FIG. 9. The nullclines of Eqs. (A1) and (A2). The shaded bands indicate where the time scales for Ψ are shortened according to Eq. (A4). This illustration is for simulation (ϵ1). The small circle displays the (constant) values of u and v at the center of the unperturbed spiral.

and (2), we take $\alpha=1$; the functions Φ, Ψ are

$$\Phi(u,v)=-\phi(u)+v, \tag{A1}$$

$$\Psi(u,v)=(-u+v)\epsilon/S(u), \tag{A2}$$

with a constant parameter $\epsilon>1$. Figure 9 illustrates the reaction functions Φ and Ψ by way of their nullclines.

The function ϕ is piecewise linear according to

$$\phi(u)=\begin{cases} -K_1u & \text{for } u<A_1 \\ K_2(u-E) & \text{for } A_1\leqslant u\leqslant A_2 \\ -K_3(u-1) & \text{for } u>A_2. \end{cases} \tag{A3}$$

The function S is piecewise constant according to

$$S(u)=\begin{cases} S_1 & \text{for } u<B_1 \\ S_2 & \text{for } B_1\leqslant u\leqslant B_2 \\ S_3 & \text{for } u>B_2. \end{cases} \tag{A4}$$

The ratios S_1/S_2 and S_3/S_2 serve to regulate, more or less independently of the other features, the amounts of time needed by the wave's recovery and plateau, respectively. The parameters A_2 and E are determined by demanding continuity of the function $\phi(u)$: $A_2=[(K_1+K_2)A_1+K_3]/(K_2+K_3)$, $E=A_2(K_1+K_2)/K_2$. In all simulations the following parameter values have been used: $K_1=4$, $K_3=15$, $A_1=0.018$, $B_1=0.01$, $B_2=0.95$, $S_2=16.5$, and $S_3=3.5$. The other parameters were varied as shown in Table I; the derived parameters are headed in brackets. The shorthand labels, such as (K.725), are not numerical quantities but stand for the simulations. The labels (ϵ1), (K.95), and (S.5) are equivalent as they denote a simulation that corresponds to the intersection of three families of points in parameter space.

In Table II we list some simple characteristics of the unperturbed spirals ($\mathbf{G}=0$), as well as our measurements and predictions for the drift velocity. Each simulation label refers to the input parameters of Table I. For each simulation we list the unperturbed period of revolution τ; the plane-wave speed of propagation c with the spiral's period, the (time-independent) value u_0 at the center of rotation, the density σ of the unperturbed spiral, as defined in Sec. IV, the observed magnitude $V=|\mathbf{V}|$ in units of $G=|\mathbf{G}|$, the observed angle $\Gamma=\angle\mathbf{GV}$ of drift, defined as positive when counterclockwise from $\mathbf{G}$ to $\mathbf{V}$, and the corresponding predicted values V_{pred}, Γ_{pred}. We also note that in each simulation the central values of u and v are equal,

$$u_0=v_0. \tag{A5}$$

This is due to our arbitrary relative normalization of u and v, see Eq. (A2), and to the fact that, in Eq. (2), we have $\partial_t v=0$ at that point. The value of u_0 is not very critical in the present paper, owing to the piecewise linear feature of the nullcline in Eq. (A1), Appendix A. In all but two of the spirals of which we were able to study the drift, we find u_0 to be located in the nullcline's middle section. In two ''supersparse'' spirals, namely, (K.725) and (K.75), the core center is totally or almost inactive, and u is extremely close to the discontinuities in the reaction functions; we are, therefore, not able to predict the corresponding two drift vectors.

All measured drifts, except in simulation (K.725), are due to the choice of convection parameter $G=0.04$; by comparison with $c\approx1$, G is a small perturbation. In (K.725) we used $G=0.01$ in order to bring down the drift velocity and thus maintain accuracy in the measurement. The drifting spirals were produced by cross stimulation with two plane pulses [4] in a square of 128×128 lattice sites, with space step$=0.4$

TABLE I. Simulation parameters.

Simulation label	K_2	$[A_2]$	$[E]$	S_1	ϵ
(K.725)	0.725	0.959	0.1173	0.5	1
(K.75)	0.75	0.958	0.1140	0.5	1
(K.775)	0.775	0.956	0.1109	0.5	1
(K.8)	0.80	0.955	0.1080	0.5	1
(K.825)	0.825	0.953	0.1053	0.5	1
(K.85)	0.85	0.952	0.1027	0.5	1
(K.875)	0.875	0.950	0.1003	0.5	1
(K.9)	0.90	0.949	0.0980	0.5	1
(K.925)	0.925	0.947	0.0958	0.5	1
(K.975)	0.975	0.945	0.0918	0.5	1
(K1)	1.00	0.943	0.0900	0.5	1
(ϵ.5)	0.95	0.946	0.0938	0.5	0.5
(ϵ.75)	0.95	0.946	0.0938	0.5	0.75
(ϵ1),(K.95),(S.5)	0.95	0.946	0.0938	0.5	1
(ϵ1.25)	0.95	0.946	0.0938	0.5	1.25
(ϵ1.5)	0.95	0.946	0.0938	0.5	1.5
(ϵ1.75)	0.95	0.946	0.0938	0.5	1.75
(ϵ2)	0.95	0.946	0.0938	0.5	2
(S2.5)	0.95	0.946	0.0938	2.5	1
(S4.5)	0.95	0.946	0.0938	4.5	1
(S6.5)	0.95	0.946	0.0938	6.5	1
(S8.5)	0.95	0.946	0.0938	8.5	1
(S10.5)	0.95	0.946	0.0938	10.5	1
(S12.5)	0.95	0.946	0.0938	12.5	1

TABLE II. Unperturbed and drift data.

Simulation label[a]	τ	c	u_0	σ	V/G	Γ (deg)	V_{pred}/G	Γ_{pred} (deg)
(K.725)	85.56	0.92	0.000	0.16	1.789	61.7	[c]	[c]
(K.75)	59.18	0.89	0.009	0.23	1.263	63.0	[c]	[c]
(K.775)	45.10	0.93	0.067	0.30	0.836	69.6	0.766	76.2
(K.8)	37.33	0.93	0.120[b]	0.37	0.585	83.7	0.624	86.8
(K.825)	32.54	0.96	0.175	0.42	0.485	96.8	0.564	84.6
(K.85)	29.25	0.99	0.215[b]	0.47	0.446	105.6	0.534	101.7
(K.875)	26.88	1.02	0.252	0.51	0.433	111.5	0.515	106.4
(K.9)	25.06	1.04	0.285[b]	0.54	0.431	115.3	0.500	110.0
(K.925)	23.68	1.08	0.315	0.58	0.433	117.9	0.493	113.4
(K.975)	21.63	1.12	0.376[b]	0.66	0.450	118.6	0.486	117.5
(K1)	20.98	1.14	0.410	0.71	0.462	116.7	0.483	118.6
(ϵ.5)	23.28	1.12	0.465	0.87	0.509	133.0	0.494	130.6
(ϵ.75)	22.27	1.10	0.401	0.73	0.445	122.2	0.482	124.2
(ϵ1),(K.95),(S.5)	22.53	1.09	0.346	0.63	0.443	118.3	0.491	115.8
(ϵ1.25)	23.39	1.08	0.299	0.55	0.445	110.9	0.514	106.0
(ϵ1.5)	24.90	1.05	0.251	0.48	0.486	102.6	0.565	94.6
(ϵ1.75)	27.44	1.04	0.195	0.41	0.561	87.5	0.681	80.5
(ϵ2)	31.94	1.03	0.122	0.35	0.770	69.4	0.985	63.3
(S2.5)	23.31	1.05	0.328	0.97	0.476	120.1	0.496	114.1
(S4.5)	26.28	1.02	0.280	1.28	0.548	123.0	0.509	107.0
(S6.5)	29.29	0.99	0.239	1.56	0.635	127.8	0.537	100.2
(S8.5)	32.18	0.96	0.205	1.81	0.815	137.5	0.561	94.3
(S10.5)	34.95	0.92	0.177	1.99	0.950	148.0	0.594	89.2
(S12.5)	37.61	0.89	0.154	2.26	1.000	166.0	0.625	84.6

[a]For parameter specification, see Table I.

[b]Interpolated value.

[c]No prediction (core nearly inactive).

and Neumann boundary conditions for u. For the unperturbed spirals the figures were 256×256 sites and a 0.2 space step. We used a first-order Euler algorithm with time step $=0.0125$ in the perturbed case and 0.003 13 in the unperturbed case. The drift velocity was obtained from the trajectory of the core. The points of that trajectory were recorded one period apart in time, as follows: The u variable was averaged over one period at every space point; as a result, the core was displayed as a low-amplitude disc, whose center defined the required trajectory point.

APPENDIX B: SHIFTED CENTERS OF ROTATION

Here we consider, in the codrifting system, the $o(G)$ correction to $u(r,\theta,t)$, which at $r=0$ can be said without loss of generality to have the component of frequency ω [also contained in Eq. (45)]:

$$(\delta u)_\omega = -u_1 r_u \cos(\omega t+\theta_u). \tag{B1}$$

We demonstrate that the fixed vector $\mathbf{r}_u$, or (r_u,θ_u), marks the rotation center for that frequency component. As a starting point, the most general nonsingular expansion of u_ω about $\mathbf{r}=0$ can be written,

$$u_\omega = m\cos(\omega t-\mu)+r[m_+\cos(\omega t+\theta-\mu_+) + m_-\cos(-\omega t+\theta-\mu_-)]+o(r^2), \tag{B2}$$

for some constants m, m_+, m_-, μ, μ_+, and μ_-, to all orders in G; we note the unperturbed values,

$$(m,m_+,m_-,\mu_+)\to(0,u_1,0,0) \text{ as } G\to0. \tag{B3}$$

Next, without looking at Eq. (B1), we define $\mathbf{r}_u$ as the rotation center for u_ω. Requiring $u_\omega=\text{const}\ (=0)$ at some point $\mathbf{r}_u$, we have from Eq. (B2),

$$m\cos(\omega t-\mu)+r_u[m_+\cos(\omega t+\theta_u-\mu_+) + m_-\cos(-\omega t+\theta_u-\mu_-)]+o(r_u^2)=0. \tag{B4}$$

In connection with Eq. (45) we have noted that the origin, $\mathbf{r}=0$ (i.e., the center of the unperturbed spiral), is chosen within an $o(G)$ distance from $\mathbf{r}_u$; this implies $r_u=o(G)$, $o(r_u^2)=o(G^2)$. Keeping only the $o(G)$ terms in Eq. (B4), we have

$$m\cos(\omega t-\mu)=-u_1 r_u\cos(\omega t+\theta_u-\mu_+). \tag{B5}$$

But at $\mathbf{r}=0$, Eq. (B2) gives

$$u_\omega(=\delta u_\omega)=m\cos(\omega t-\mu). \tag{B6}$$

Together with Eq. (B5), this leads to Eq. (B1).

An entirely similar argument where ω is replaced by its integer multiples, leads to vanishing harmonics in the $o(G)$ corrections:

$$(\delta u)_{2\omega}=(\delta u)_{3\omega}=\ \ldots\ =0. \tag{B7}$$

Here again we make use of the unperturbed spiral, where nonsingularity at the center, combined with rigid rotation, leads to the components of frequencies 2ω, 3ω, ... being of order r^2, r^3, ... in the r expansion. Thus, in Eq. (B3) we have unperturbed values,

$$(m,m_+,m_-)\rightarrow(0,0,0) \quad \text{as} \quad G\rightarrow 0, \tag{B8}$$

leading to Eq. (B7). [Each harmonic has its own shifted rotation center, but this does not affect the argument.]

Finally, we derive for the zero-frequency component, or time average, at $\mathbf{r}=0$:

$$\langle \delta u(0)\rangle = o(G^2). \tag{B9}$$

We start from the fact that $\langle \delta u(\mathbf{r}_u)\rangle = o(G^2)$, by the argument that yielded Eq. (44). But we have

$$u(0)=u(\mathbf{r}_u)-\mathbf{r}_u\cdot\boldsymbol{\nabla}u(\mathbf{r}_u)+o(r_u^2) \tag{B10}$$

or, since $r_u=o(G)$,

$$\delta u(0)=\delta u(\mathbf{r}_u)-\mathbf{r}_u\cdot\boldsymbol{\nabla}[u(0)]_{G=0}+o(G^2). \tag{B11}$$

Using $\langle \boldsymbol{\nabla}u(0)\rangle_{G=0}=0$, we have

$$\langle \delta u(0)\rangle = \langle \delta u(\mathbf{r}_u)\rangle + o(G^2), \tag{B12}$$

or Eq. (B9) as claimed.

In conclusion, the present appendix makes the following statements: (a) The $o(G)$ correction to u at $\mathbf{r}=0$ is given by its fundamental-frequency term only,

$$\delta u=(\delta u)_\omega; \tag{B13}$$

(b) furthermore, its time behavior at that point merely expresses a spatial shift in the rotation center of u_ω.

These results are applicable to any other spiral-wave variables as well, such as δv or any of the variables (46)–(50). We note that the system is translationally invariant. Therefore, one of these variables, for example δu itself, can always be chosen to have an unshifted center; but if $\mathbf{r}_u=0$ then in general one must have $\mathbf{r}_v\neq 0$, etc.

APPENDIX C: CIRCULAR AND RECTANGULAR-HYPERBOLIC LOCI

Here we convert Eq. (73) into a circular locus in the **V** plane and Eq. (76) into a rectangular-hyperbolic locus. We also determine which of the intersections of these two curves is the ''physical'' one.

Equation (73). Eliminating $\mathbf{r}_C$ with the help of Eq. (66), we obtain from Eq. (73),

$$r_B\cos(\chi_B-\chi_C+2\psi+\theta_B-\Gamma)=-(V/\omega)\sin\chi_C\cos\chi_B. \tag{C1}$$

On the other hand, Eq. (53), with $\mathbf{r}_A=0$ and $\mathbf{r}_C$ eliminated as above, gives

$$r_B\cos(\omega t-\chi_B+\theta_B)-\frac{VP\partial_v\Phi\sin\psi}{B\omega^2}\cos(\omega t+\Gamma-2\psi)$$
$$=-\frac{u_1}{B}[V\cos(\omega t+\Gamma)+G\cos\omega t]. \tag{C2}$$

Taking $\omega t=2\chi_B-\chi_C+2\psi-\Gamma$ and subtracting Eq. (C1) gives

$$\frac{V}{G}\left[\frac{B}{u_1\omega}\sin\chi_C\cos\chi_B+\frac{P\partial_v\Phi\sin\psi}{u_1\omega^2}\cos(2\chi_B-\chi_C)\right.$$
$$\left.-\cos(2\chi_B-\chi_C+2\psi)\right]$$
$$=\cos(2\chi_B-\chi_C+2\psi-\Gamma). \tag{C3}$$

We next use Eqs. (40) and (22) for P/u_1, Eq. (35) for B/u_1, and Eq. (36) to eliminate the reaction functions. Equation (C3) eventually reduces to

$$\frac{V}{G}(\sin 2\chi_B\sin\chi_C+\cos\Gamma_0)=-\cos(\Gamma-\Gamma_0), \tag{C4}$$

where

$$\Gamma_0=2\chi_B-\chi_C+2\psi-\pi. \tag{C5}$$

In the **V** plane, Eq. (C4) represents a circle that passes through the origin, and whose center has angular coordinate Γ_0.

Equation (76). Taking $\omega t=\theta_C+\pi/2$ in Eq. (C2) makes its first term vanish by Eq. (76); Eq. (C2) now reads

$$\frac{V}{G}\left[\frac{P\partial_v\Phi\sin\psi}{u_1\omega^2}\sin(\theta_C+\Gamma-2\psi)-\sin(\theta_C+\Gamma)\right]=\sin\theta_C. \tag{C6}$$

Using Eq. (66) for θ_C, and successively eliminating P and the reaction functions by means of Eqs. (40), (22), and (36), we reduce Eq. (C6) to

$$\frac{V}{G}[H\sin(2\Gamma+\chi_C-4\psi)-\sin(2\Gamma+\chi_C-2\psi)]$$
$$=\sin(\Gamma+\chi_C-2\psi), \tag{C7}$$

where H is a known constant,

$$H=\frac{\cos\chi_B\sin\chi_C}{\sin(\chi_C-\chi_B)}. \tag{C8}$$

In the **V** plane, Eq. (C7) represents a rectangular hyperbola that passes through the origin.

Selecting the intersection. Between the circle and the hyperbola we have, in general, four intersections, one of which is at $\mathbf{V}=0$. We are unable to exclude the later by a rigorous argument. However, by continuity $\mathbf{V}=0$ is extremely implausible. Indeed, that intersection never moves as the model's parameters are being varied, which would imply zero drift in a finite volume of parameter space. Of the three re-

maining intersections we exclude two by inequalities that originate from the unperturbed data, as follows.

From Eq. (73), and using $\cos\chi_B>0$, we have

$$\cos(\theta_B-\theta_C+\chi_B)>0, \tag{C9}$$

or, eliminating θ_B and θ_C by using Eqs. (66) and (76),

$$\cos[2(\Gamma+\chi_C-\chi_B-2\psi)]<0. \tag{C10}$$

A second inequality results from the observation that both sequences **ABC** and **abc** have the same chirality. This results in $\sin(\theta_C-\theta_B)>0$, or eliminating θ_B and θ_C as above,

$$\sin[2(\Gamma+\chi_C-\chi_B/2-2\psi)]<0. \tag{C11}$$

The pair of restrictions expressed by Eqs. (C10) and (C11) always leave us with a single predicted drift in the cases considered. To sum up this appendix: the pair of Eqs. (C4) and (C7), together with inequalities (C10) and (C11) constitute our prediction for the normalized drift velocity $(V/G,\Gamma)$.

[1] *Waves and Patterns in Chemical and Biological Media*, edited by H. L. Swinney and V. I. Krinsky (Elsevier, Amsterdam, 1991), Chaps. 1–3.

[2] Chaos **8** (1) (1998).

[3] J. M. Davidenko, A. M. Pertsov, R. Salomonsz, W. Baxter, and J. Jalife, Nature (London) **355**, 349 (1992).

[4] A. M. Pertsov, J. M. Davidenko, R. Salomonsz, W. T. Baxter, and J. Jalife, Circ. Res. **72**, 631 (1993).

[5] V. G. Fast and A. M. Pertsov, J. Cardiovasc. Electrophysiol. **3**, 255 (1992).

[6] K. I. Agladze and P. DeKepper, J. Phys. Chem. **96**, 5239 (1992).

[7] O. Steinbock, J. Schütze, and S. C. Müller, Phys. Rev. Lett. **68**, 248 (1992).

[8] G. S. Skinner and H. L. Swinney, Physica D **48**, 1 (1990).

[9] A. T. Winfree, Chaos **1**, 303 (1991).

[10] A. M. Pertsov and Ye. A. Yermakova, Biofizika **33**, 338 (1988) [Biophysics (Engl. Trans.) **33**, 364 (1988)].

[11] A. P. Muñuzuri, M. Gómez-Gesteira, V. Pérez-Muñuzuri, V. I. Krinsky, and V. Pérez-Villar, Phys. Rev. E **48**, R3232 (1993).

[12] V. Krinsky, E. Hamm, and V. Voignier, Phys. Rev. Lett. **76**, 3854 (1996).

[13] D.-F. Ding, Physica D **32**, 471 (1988).

[14] V. N. Biktashev and A. V. Holden, Chaos Solitons Fractals **5**, 575 (1995).

[15] I. V. Biktasheva, Yu. E. Elkin, and V. N. Biktashev, Phys. Rev. E **57**, 2656 (1998).

[16] A. Pertsov and M. Vinson, Philos. Trans. R. Soc. London, Ser. A **347**, 687 (1994), see especially pp. 690 and 691.

[17] J. F. Spear, E. L. Michelson, and E. N. Moore, Circ. Res. **53**, 176 (1983).

[18] O. Berenfeld and A. M. Pertsov (unpublished).

[19] J. P. Keener and J. J. Tyson, SIAM (Soc. Ind. Appl. Math.) Rev. **34**, 1 (1992).

[20] A. V. Panifilov, A. N. Rudenko, and V. I. Krinsky, Biofizika **31**, 850 (1986) [Biophysics (Engl. Trans.) **31**, 926 (1986)].

[21] M. Vinson, S. Mironov, S. Mulvey, and A. M. Pertsov, Nature (London) **386**, 477 (1997).